ChemComm

COMMUNICATION

View Article Online
View Journal | View Issue

Cite this: *Chem. Commun.*, 2025, **61**, 14366

Received 25th June 2025,
Accepted 13th August 2025

DOI: 10.1039/d5cc03591k

rsc.li/chemcomm

Side-chain dependent direct *vs.* indirect photoresponse in hydrazone-based supramolecular polymers

Subhankar Paul* and Debangshu Chaudhuri *

The aggregate-to-aggregate photoconversion pathway, *via* monomers or not (indirect *vs.* direct), depends on a suitable balance between intermolecular interactions and accessible free space for isomerisation within the aggregate. We show that introducing fluorophilic interactions by side chain engineering in a hydrazone-based system can alter the photoconversion mechanism from indirect to direct, accompanied by distinct photophysical, morphological and mechanical changes.

Photoresponsive supramolecular polymerization offers a promising way to incorporate stimuli-responsiveness in assembled nanostructures, by way of introducing a light-induced structural change in the molecular building blocks.[1,2] Light-driven conformational/structural changes in the building blocks can affect the free energy of molecular association, and thus establish a new self-assembly equilibrium for the irradiated building blocks, which may result in assembly reorganization[2] or disassembly.[2,3] Assembly photoconversion in solution can be achieved in two distinct ways: direct[2,4] and indirect.[5] In direct photoconversion, molecular building blocks embedded within the assembled structure isomerize and trigger an *in situ* change in the packing arrangement, often leading to topographical changes. Such dynamic control over topography can be crucial in biomedical applications, where bacterial growth[6] and enzyme activity[7] show dependence on the surface characteristics of the material. In contrast, an indirect photoconversion proceeds *via* an intermediate monomeric state. Strain induced in the assembled structure by way of photoisomerisation causes disassembly, and the free monomers thus produced reassemble into a new/transformed structure. Such indirect photoconversions may be associated with large morphological changes.[5] A direct photoisomerization in the assembled state is dictated by how strongly the rotating unit of the molecule is held/immobilized by the noncovalent interactions, as well as the available free space to permit any structural change associated with the isomerization. Only a suitable balance of these two can facilitate a direct photoconversion over an indirect one.

Hydrazone-based photoswitches[8] are a suitable candidate for designing photoresponsive assemblies, as it offers the flexibility to separately design the stator and the rotor part (Fig. 1a), high thermal half-lives[9] and pH responsiveness.[10] Aprahamian and coworkers have worked extensively on hydrazone-based photoswitches, elucidating the tunability of electronic and photophysical properties by modifying the stator and rotor part.[11] We design **Hy-R** (R = Bu/F, see Fig. 1a) by introducing an amide linkage to the stator part with the expectation that its self-assembly in solution will be guided by directional intermolecular H-bonding between the amide groups, while the rotor part remains relatively free to undergo isomerization. Structural investigations show that the self-assembly of **HyBu** and **HyF** are primarily driven by H-bonding and weak n → π* interactions, involving primarily the stator part. In addition to these, replacing the butyl sidechain in **HyBu** with a 1*H*,1*H*-perfluorobutyl group (in **HyF**) introduces weak fluorophilic interactions.[12] This seemingly small difference in the packing interactions has a significant bearing on the photoconversion pathway, which changes from indirect (**HyBu**) to direct (**HyF**). The

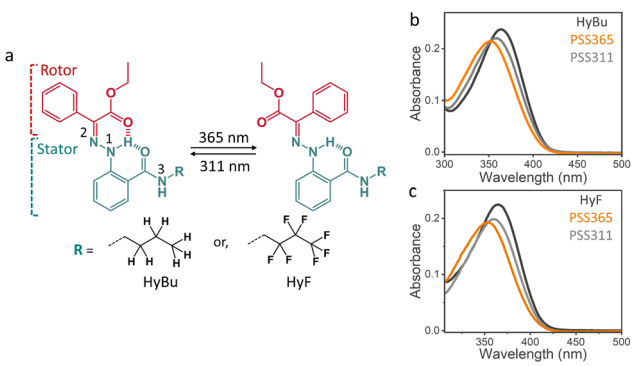

Fig. 1 (a) Molecular structures of the *Z*-isomers of **HyF** and **HyBu**. Light induced *Z*/*E* isomerisation. N atoms are numbered to aid discussion. Changes in absorbance spectra of (b) **HyBu** and (c) **HyF** on forward (365 nm) and backward (311 nm) photoirradiation in ethanol (15 μM).

Department of Chemical Sciences, Indian Institute of Science Education and Research (IISER) Kolkata, Mohanpur-741246, India.
E-mail: dchaudhuri@iiserkol.ac.in

contrasting effects of the assembly photoconversion mechanism on optical, morphological and mechanical properties have been investigated.

HyBu and **HyF** were synthesized in the *Z*-form following the method described in the SI (scheme S1 and Fig. S1–S6). Fig. 1b and c present the absorbance spectra of the hydrazone derivatives in the molecularly dissolved state in ethanol. The molecular absorption spectra of both hydrazone derivatives present a broad, featureless peak at 365 nm (λ_{max}) that corresponds to the $\pi \rightarrow \pi^*$ transition. It is due to the aromatic unit with extended conjugation through intramolecular H-bonding in *Z*-isomers (Fig. 1a).[13] Under 365 nm irradiation, the absorption maximum shows a blue shift to 351 nm, and a photostationary state is achieved after 2 min of irradiation (Fig. 1). The observed blue shift is consistent with the reduction in the extended π-conjugation upon *Z*- to-*E* isomerization, which disrupts the intramolecular N_1–H···O=C_{ester} H-bonding and results in a loss of coplanarity.[9] Despite a strong overlap between the absorption spectra of *Z* and *E* isomers, it is possible to partially achieve the back (*E*-to-*Z*) isomerization under 311 nm photoirradiation (Fig. 1). These photoisomerisation events can be further confirmed and quantified by ^{1}H NMR spectroscopy. Fig. S7a–c show clear changes in the chemical shift values of the N_1–H proton from 13.80 to 11.46 ppm for **HyBu** (and from 13.69 to 11.24 ppm, for **HyF**) upon photoisomerization. From the ^{1}H NMR spectra, we estimate a *Z*-to-*E* ratio of 40 : 60 upon 365 nm irradiation (PSS365). Likewise, upon 311 nm irradiation, the photostationary state (PSS311) shows a 66 : 34 *Z* to *E* ratio.

Self-assembly of the hydrazone derivatives was carried out by injecting a concentrated (4.7 mM) ethanolic solution of the monomers into water. The optical absorbance spectra of **HyBu** exhibit a bathochromic shift from 365 to 375 nm (see Fig. S9a), along with a spectral broadening that indicates possible slipped-stacking of the hydrazone chromophores in the assembled state (**HyBu-Agg**). Slipped molecular packing in **HyBu-Agg** is also supported by single-crystal x-ray diffraction (SCXRD), presented later. In contrast, the absorption spectrum of the assembled **HyF** (**HyF-Agg**) shows no such shift in the absorption maximum, but only a considerable hypochromism and spectral broadening (Fig. S9b). While monomeric **HyBu** and **HyF** are both non-emissive, their assemblies show a weak photoluminescence at ∼465 nm, with photoluminescence quantum yields (Φ_{PL}) of 0.3–0.4% (Fig. S9). Such aggregation-induced emission (AIE) may be attributed to rigidification of the molecular conformation in the assembled state.[14]

Fig. 2a and b summarize the photoresponse of the assembled **HyBu** and **HyF** towards 365 nm irradiation. In the case of **HyBu-Agg**, photoirradiation results in a significant blue-shift in the absorbance maximum, from 375 to 349 nm with a clear isosbestic point at 357 nm (see Fig. 2a). Instead, photoirradiation of **HyF-Agg** causes only a decrease in the absorbance at λ_{max}, without any spectral shift. A new absorption band however appears at 463 nm, with an isosbestic point at 426 nm (see Fig. 2b). There are also corresponding changes in the PL characteristics of the photoirradiated aggregates. While photoisomerization of **HyBu-Agg** results in a 33%

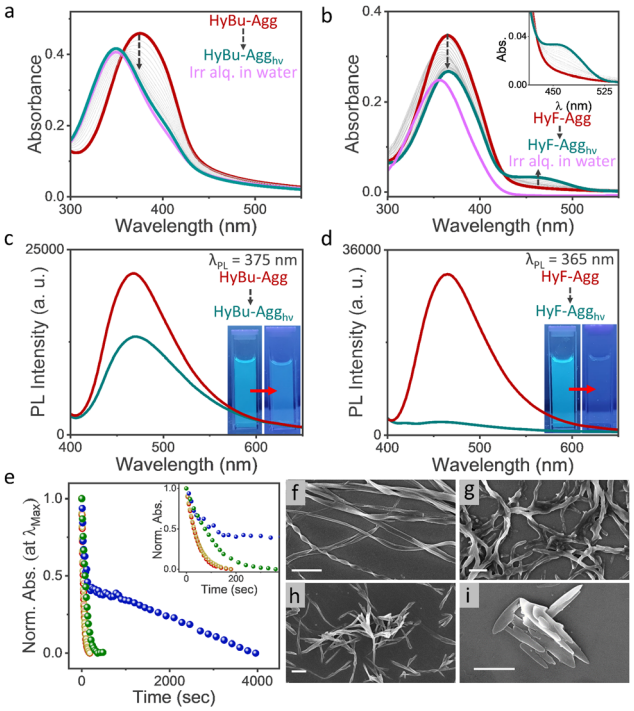

Fig. 2 Changes in absorbance spectra of (a) **HyBu** and (b) **HyF** aggregates in water upon 365 nm irradiation. In each case, the spectrum of the isomerized monomer (*Z* : *E* = 40 : 60) assembled in water is shown for comparison (violet line). (c) and (d) Corresponding changes in aggregate PL spectra upon photoirradiation. Inset shows before and after PL images of aggregate solutions. (e) Semi-logarithmic plot of absorbance at the respective λ_{max} with time shows differences in photoconversion kinetics: **HyBu** monomer (yellow), **HyF** monomer (red), **HyBu-Agg** (green) and **HyF-Agg** (blue). The inset shows a magnified view of the kinetics in the early stages. FESEM images of aggregates before and after 365 nm irradiation: (f) **HyF-Agg**, (g) **HyF-Agg$_{hν}$**, (h) **HyBu-Agg** and (i) **HyBu-Agg$_{hν}$**. Scale bar: 1 μm.

decrease in the PL intensity (Fig. 2c), **HyF-Agg** shows a near-complete PL quenching (see Fig. 2d). Interestingly, the kinetics of the photoresponse are very different for the two aggregated hydrazones. Fig. 2e compares the rate of photoresponse for **HyBu-Agg** and **HyF-Agg**, presented in terms of the relative change in the absorbance at the respective λ_{max}. The plot highlights the contrasting nature of the two isomerisation pathways. Quite expectedly, the photoisomerization kinetics of monomeric **HyBu** and **HyF** are identical. **HyBu-Agg** follows a marginally slower photoconversion kinetics (Fig. 2e, green circles). Similar photoisomerization rates of **HyBu-Agg** and monomeric **HyBu** provide compelling evidence in favour of an indirect photoconversion, where aggregate reorganization happens by way of a disassembly-reassembly mechanism. The corresponding photostationary state (**HyBu-Agg$_{hν}$**) is achieved with a *Z*-to-*E* ratio of 65 : 35, as estimated from the ^{1}H NMR study (see Fig. S11). In sharp contrast, the **HyF-Agg** photoconversion kinetics presents two distinct kinetic stages: a faster process with a rate comparable to that of the monomers, and a much slower process (Fig. 2e, blue circles). Furthermore, ^{1}H NMR spectroscopy reveals only 5% $Z \rightarrow E$ isomerization even after 120 min irradiation (Fig. S12). This is unlike **HyBu-Agg** where 35% $Z \rightarrow E$ conversion can be achieved within 4 min

of irradiation under identical conditions. A considerably slower kinetics and low photoconversion yield in **HyF-Agg** indicates photoisomerization of the aggregate-bound **HyF** molecules, and consequently a direct aggregate-to-aggregate photoconversion. To further establish the hypothesis of direct *vs.* indirect photoconversion, we carried out self-(co)assembly of a mixture of *Z*- and *E*- monomers in water (see SI). Fig. 2b and Fig. S13 present the absorption spectrum of premixed 95 : 5 (*Z* : *E*) **HyF** in water. The absorption maximum is slightly shifted to 363 nm, but the 463 nm band is conspicuously absent, even when the monomer mixture with higher fraction of *E*-isomer (*Z* : *E* = 40 : 60) is used. Therefore, we can conclude that the 463 nm band is the characteristic absorption feature of **HyF-Agg** that has undergone a direct aggregate-to-aggregate photoconversion. On the other hand, adding an ethanolic solution of premixed 40 : 60 (*Z* : *E*) **HyBu** into water shows an identical absorption spectrum as that of photoirradiated **HyBu-Agg**, confirming an indirect aggregate-to-aggregate photoconversion (Fig. 2a and Fig. S13). We note that **HyBu-Agg**$_{h\nu}$ can be partially reversed back to the initial state upon 311 nm irradiation, and the reversibility could be demonstrated over multiple cycles of photoirradiation (Fig. S14). In contrast, **HyF-Agg**$_{h\nu}$ remains unresponsive to 311 nm irradiation (Fig. S15).

Changes in aggregate morphology are also consistent with the expectation of direct *vs.* indirect photoconversion. FESEM images of **HyF-Agg** show an entangled fibrillar network, with fibres extending to several microns in length (Fig. 2f and Fig. S16). In certain cases, individual fibers also exhibit a helical twist. Upon photoirradiation, **HyF-Agg**$_{h\nu}$ also shows fibrillar morphology but with significantly altered surface topography (Fig. 2g and Fig. S16). FESEM images of **HyBu-Agg** too reveal a 1D fibrillar morphology (Fig. 2h and Fig. S17). But a drastic change in the dimension is observed upon photoirradiation. The 1D fibers transform into shorter, flattened rice-shaped nanostructures (Fig. 2i and Fig. S17). These observed changes in dimension of the assembled nanostructures are also reflected in Dynamic light scattering (DLS) measurements. The hydrodynamic diameter (D_H) of **HyF-Agg** remains unchanged (~800 nm) before and after photoirradiation, whereas a decrease from 600 nm to 230 nm is observed for **HyBu-Agg** (Fig. S18). Once again, the photoreversibility of **HyBu-Agg** could be confirmed by demonstrating the regeneration of the fibrillar morphology in FESEM, as well as an increase in particle size (D_H) in DLS (Fig. S17 and S18).

Fig. 3a presents the pXRD patterns of the **HyBu** and **HyF**-aggregates (see SI for details). An SCXRD experiment was carried out on **HyBu** single crystals grown from a chloroform-ethanol (2 : 1 v/v) mixture, and the diffraction data was analyzed to solve the crystal structure. The pXRD pattern simulated from the **HyBu** crystal structure data matches well with the experimental pXRD pattern of **HyBu-Agg** grown from aqueous solution, allowing us to unambiguously determine the molecular packing arrangement in the assembled **HyBu-Agg**. SCXRD analysis shows that **HyBu** crystallizes into a triclinic ($P\bar{1}$) space group (Table S1 and CCDC 2432753). Interestingly, the **HyBu** crystal is a conformational isomorph. The two molecules in the asymmetric unit are conformationally distinct, with respect to

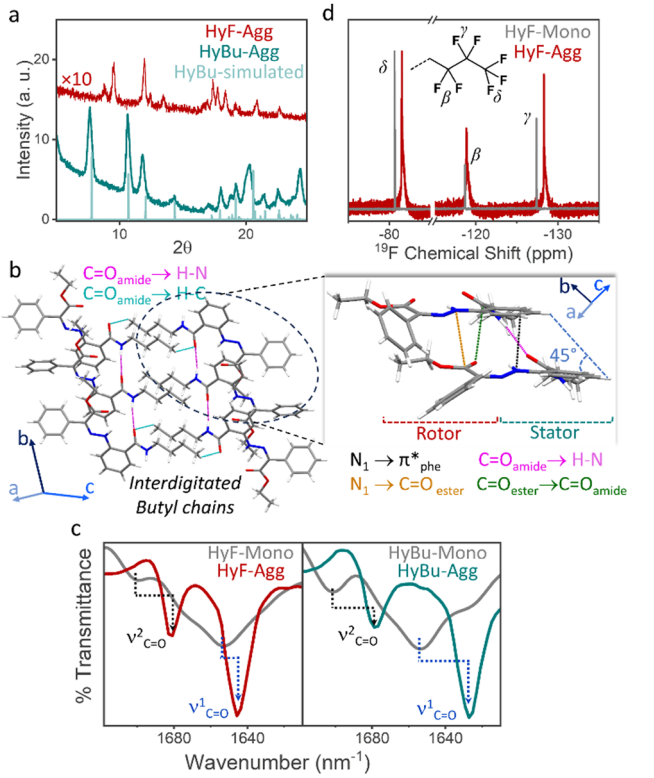

Fig. 3 (a) pXRD pattern of **HyF** and **HyBu** aggregates. The simulated pXRD pattern of the **HyBu** single crystal matches with that of **HyBu-Agg**. (b) Molecular packing in the **HyBu** single crystal shows amide H-bonding along the *b*-axis and butyl chain interdigitation along the *c*-axis. (c) FTIR spectra show changes in carbonyl stretching frequencies for amide ($\nu^1_{C=O}$) and ester ($\nu^2_{C=O}$) groups upon aggregation. (d) Changes in ^{19}F NMR chemical shift upon **HyF** aggregation in 2 : 1 D_2O–EtOH.

the orientation of the phenyl group in the rotor part (Fig. S19). A pair of intramolecular N_1–H···O=$C_{(ester/amide)}$ H-bonding interactions hold the rotor and stator part in an almost planar geometry, and help to achieve an extended electronic conjugation (Fig. S20a). The planarity also allows **HyBu** molecules to stack in a slipped manner along the *b*-axis, promoting 1D columnar growth. The major structure-directing interactions are amide H-bonding with alternating H-bonding distances of 2.068 and 2.139 Å. Other weak n → π* interactions, such as N_1 → phenyl, N_1 → C=O_{ester} and C=O_{ester} → C=O_{amide} are also operative (Fig. 3b and Fig. S20b). The slip-angle and the interplanar distance are 45° and 3.39 Å, respectively. Interestingly, adjacent columns grow in an antiparallel fashion, interacting weakly through interdigitated butyl chains and C=O_{amide}···H–C H-bonding. It is evident that while the stator part of the **HyBu** molecule is involved in stronger noncovalent interactions (amide H-bonding *etc.*), the rotor part too participates in n → π* interactions (N_1 → C=O_{ester} and C=O_{ester} → C=O_{amide}), as a result of which isomerisation can destabilize the assembled state.

Unlike **HyBu**, we could not grow single crystals of **HyF**. However, the pXRD pattern of **HyF-Agg** exhibits considerably less intense diffraction peaks, suggesting poorer crystallinity (Fig. 3a). FTIR spectroscopy gives valuable insight into the comparative strengths of H-bonding and n → π* interactions

in the two aggregates (Fig. 3c). The carbonyl stretching frequencies for amide ($\nu^1_{C=O}$) and ester ($\nu^2_{C=O}$) groups for monomeric **HyBu** and **HyF** appear at 1653 and 1700 cm^{-1}, respectively. In **HyBu-Agg**, $\nu^1_{C=O}$ and $\nu^2_{C=O}$ are red-shifted to 1627 cm^{-1} and 1677 cm^{-1}, respectively. This can be correlated with the crystal structure that shows $C{=}O_{amide}$ participating in intermolecular H-bonding and $C{=}O_{ester}$ in n → π* interaction ($C{=}O_{ester}$ → $C{=}O_{amide}$). In contrast, the corresponding FTIR shifts are relatively lower for **HyF-Agg**; $\nu^1_{C=O}$ appears at 1645 cm^{-1} and $\nu^2_{C=O}$ is at 1681 cm^{-1}. That a weakly bound **HyF-Agg** survives the strain-caused photoisomerization while a more strongly bound **HyBu-Agg** undergoes disassembly may seem counterintuitive. This apparent anomaly may be explained by considering both the rotor and stator parts. Relatively weaker H-bonding and n → π* interactions in the rotor part of **HyF-Agg** may lead to a less intimate packing, and consequently more available space to accommodate photoisomerization-induced strain. We investigate the role of the stator part in stabilizing the aggregate structure. The solution-state ^{19}F NMR spectrum of monomeric **HyF** (Fig. 3d) shows three distinct ^{19}F resonances corresponding to different F atoms in the R_f chain (see inset to Fig. 3d), assigned as F_β (−118.7 ppm), F_γ (−127.4 ppm) and F_δ (−80.7 ppm). In **HyF-Agg**, F_γ and F_δ are strongly shielded and the peaks appear at −128.3 and −81.5 ppm, while F_β registers a negligible shift. The relative magnitude of shielding indicates the extent of penetration of the interdigitating R_f chains, which permits strong interactions between F_γ and F_δ atoms but leaves the F_β largely unaffected. It is conceivable that F···F interactions in the stator part help in stabilizing the aggregate structure against photoisomerization-induced strain, preventing disassembly and leading to a direct aggregate-to-aggregate photoconversion.

Next, we present the macroscopic manifestation of the photoresponsiveness in **HyBu** and **HyF** assemblies. At a higher concentration (c = 2 mg mL^{-1}), both **HyBu** and **HyF** form blue-emissive hydrogels (Fig. S21 and S22). Upon photoirradiation with 365 nm light, **HyF** hydrogel shows a distinct color change from white to yellow (inset to Fig. S23a), along with PL quenching. These observed changes are similar to that of solution state **HyF-Agg** (see Fig. S21). On the other hand, **HyBu** hydrogel shows a considerable change in the physical appearance. Upon photoirradiation, a significant amount (∼25%) of water is expelled from the gel, causing its partial disintegration (Fig. S23b inset and see SI for details). These differences in their physical appearance are also supported by dynamic rheological studies (Fig. S23 and S24). The **HyF** gel shows closely similar stiffness to that of **HyBu** gel, with comparable values of storage modulus and yield stress. Both the gels are significantly weakened upon photoirradiation, with **HyBu** recording a 78% reduction in yield stress (90 to 20 pa) and 50% reduction for HyF (110 to 55 pa). This may be attributed to a greater degree of isomerization in the **HyBu** aggregates, such that heterogeneity (E/Z ratio) results in weaker co-assembly. Incidentally, the viscoelastic nature of **HyBu** gel can be partially regained upon 311 nm photoirradiation, but each cycle of forward and reverse photoisomerization results in a steady decline in the yield stress (Fig. S25).

In conclusion, we have demonstrated a crucial concept of a photoresponsive aggregate-to-aggregate transition pathway in a simple way by introducing fluorophilic interaction by side chain engineering in a hydrazone-based system. Structural analysis like SCXRD, FT-IR and ^{19}F NMR reveals that it is fluorophilic interaction normal to the growth axis that helps in binding the **HyF** molecules more firmly in the aggregate than in **HyBu** and also provides relatively more free space in between the embedded molecules within the aggregate and allows *in situ* photoisomerization. Along with spectroscopic and microscopic techniques, this distinct photoconversion pathway can also be realized mechanically.

DC acknowledges IISER Kolkata for financial support. SP thanks CSIR for the fellowship, and S. Gayen and Prof. C. M. Reddy, IIT Hyderabad, for help in solving the crystal structure.

Conflicts of interest

There are no conflicts to declare.

Data availability

Data supporting this article have been included as part of the SI. Supplementary information available: Material and methods, synthesis and characterization and additional figures. See DOI: https://doi.org/10.1039/d5cc03591k

CCDC 2432753 contains the supplementary crystallographic data for this paper.[15]

References

1 F. Xu and B. L. Feringa, *Adv. Mater.*, 2023, **35**, 2204413.
2 (*a*) Y. Kitamoto, *et al.*, in *Photoactive Functional Soft Materials: Preparation, Properties, and Applications*, ed. Q. Li, Wiley-VCH, Weinheim, 2019, pp. 45–90; (*b*) Q. Zhang, *et al.*, *Adv. Opt. Mater.*, 2019, **7**, 1900033.
3 J. W. Fredy, *et al.*, *PNAS*, 2017, **114**, 11850–11855.
4 (*a*) T. Muraoka, *et al.*, *J. Am. Chem. Soc.*, 2008, **130**, 2946–2947; (*b*) S. Yagai, *et al.*, *Chem. – Eur. J.*, 2012, **18**, 2244–2253; (*c*) L. Li, *et al.*, *Angew. Chem., Int. Ed.*, 2007, **46**, 5873–5876; (*d*) B. Adhikari, *et al.*, *Nat. Commun.*, 2017, **8**, 15254; (*e*) D.-H. Qu, *et al.*, *Adv. Opt. Mater.*, 2022, **10**, 2101267; (*f*) W. Bei, *et al.*, *Macromol. Rapid Commun.*, 2018, **39**, 1700880.
5 (*a*) X. Yan, *et al.*, *PNAS*, 2014, **111**, 8717–8722; (*b*) O. Vybronyi, *et al.*, *Angew. Chem., Int. Ed.*, 2021, **60**, 25872–25877; (*c*) J. Xu, *et al.*, *Angew. Chem., Int. Ed.*, 2013, **52**, 9738–9742; (*d*) Y. Cai, *et al.*, *J. Am. Chem. Soc.*, 2016, **138**, 2219–2224.
6 H. Assender, *et al.*, *Science*, 2002, **297**, 973–976.
7 J. E. P. Brouns and P. Y. W. Dankers, *Biomacromolecules*, 2021, **22**, 4–23.
8 B. Shao and I. Aprahamian, *Chem*, 2020, **6**, 2162–2173.
9 H. Qian, *et al.*, *J. Am. Chem. Soc.*, 2017, **139**, 9140–9143.
10 X. Su and I. Aprahamian, *Org. Lett.*, 2011, **13**, 30–33.
11 B. Shao, *et al.*, *J. Am. Chem. Soc.*, 2019, **141**, 8364–8371.
12 (*a*) H. Ariam, *et al.*, *Chem. Commun.*, 2020, **56**, 15619–15622; (*b*) N. Sasaki, *et al.*, *Nat. Commun.*, 2020, **11**, 3578.
13 S. M. Landge, *et al.*, *J. Am. Chem. Soc.*, 2011, **133**, 9812–9823.
14 J. Mei, *et al.*, *Chem. Rev.*, 2015, **115**, 11718–11940.
15 S. Paul and D. Chaudhuri, CCDC 2432753: Experimental Crystal Structure Determination, DOI: 10.5517/ccdc.csd.cc2mngxp.